Temperature Dependence of the Epidermal Growth Factor Receptor Signaling Network Can Be Accounted for by a Kinetic Model†

Gisela Moehren,‡ Nick Markevich,‡ Oleg Demin,‡,§ Anatoly Kiyatkin,‡ Igor Goryanin,|| Jan B. Hoek,‡ and Boris N. Kholodenko*,‡

Department of Pathology, Anatomy, and Cell Biology, Thomas Jefferson University, 1020 Locust Street, Philadelphia, Pennsylvania 19107, A. N. Belozersky Institute of Physico-Chemical Biology, Moscow State University, Moscow, Russia, and GlaxoSmithKline, Stevenage, U.K.

Received July 19, 2001; Revised Manuscript Received October 30, 2001

ABSTRACT: Stimulation of isolated hepatocytes with epidermal growth factor (EGF) causes rapid tyrosine phosphorylation of the EGF receptor (EGFR) and adapter/target proteins, which was monitored with 1 and 2 s resolution at 37, 20, and 4 °C. The temporal responses detected for multiple signaling proteins involve both transient and sustained phosphorylation patterns, which change dramatically at low temperatures. To account quantitatively for complex responses, we employed a mechanistic kinetic model of the EGFR pathway, formulated in molecular terms as cascades of protein interactions and phosphorylation and dephosphorylation reactions. Assuming differential temperature dependencies for different reaction groups, such as SH2 and PTB domain-mediated interactions, the EGFR kinase, and the phosphatases, good *quantitative* agreement was obtained between computer-simulated and measured responses. The kinetic model demonstrates that, for each protein−protein interaction, the dissociation rate constant, k_{off}, strongly decreases at low temperatures, whereas this decline may or may not be accompanied by a large decrease in the k_{on} value. Temperature-induced changes in the maximal activities of the reactions catalyzed by the EGFR kinase were moderate, compared to such changes in the V_{max} of the phosphatases. However, strong changes in both the V_{max} and K_m for phosphatases resulted in moderate changes in the V_{max}/K_m ratio, comparable to the corresponding changes in EGFR kinase activity, with a single exception for the receptor phosphatase at 4 °C. The model suggests a significant decrease in the rates of the EGF receptor dimerization and its dephosphorylation at 4 °C, which can be related to the phase transition in the membrane lipids. A combination of high-resolution experimental monitoring and molecular level kinetic modeling made it possible to quantitatively account for the temperature dependence of the integrative signaling responses.

Epidermal growth factor receptor (EGFR)[1] belongs to a large family of receptor tyrosine kinases involved in many regulated cellular processes, including cell survival and apoptosis, proliferation, and differentiation. Binding of epidermal growth factor (EGF) or transforming growth factor α to EGFR causes receptor dimerization and rapid activation of its intrinsic tyrosine kinase followed by autophosphorylation of multiple tyrosine residues in the cytoplasmic domain. Receptor phosphorylation creates docking sites for cytoplasmic target proteins that possess Src homology 2 (SH2) or phosphotyrosine-binding (PTB) domains, such as growth factor receptor binding protein 2 (Grb2), src homology and collagen domain protein (Shc), phospholipase C-γ (PLCγ), and phosphatidylinositol 3-kinase (p85-PI3K) (see, e.g., refs *1*−*4*). Activation and tyrosine phosphorylation of these proteins lead to a further propagation of the signal through multiple interacting pathways including the SOS/Ras/MAPK, PLCγ, and PI3K pathways (*5*−*7*).

The integrated cellular response to EGF stimulation is an output of a complex interplay of multiple protein interactions and phosphorylation and dephosphorylation reactions. The time course of EGFR autophosphorylation appears to be important for activation of multiple downstream responses, yet it itself depends on the kinetic behavior of an entire pathway (*8*, *9*). Although a large body of data describes EGFR signaling at the molecular level, the control of the signal transfer at the systems level remains poorly understood. A careful examination of the influence of multiple factors requires a quantitative framework for a description of the EGFR signaling network. Recently, we developed a comprehensive kinetic model of EGFR-mediated signaling that accounted for experimentally observed response patterns (*10*). Experimental data on isolated hepatocytes demonstrated

† This work was supported by Grants GM59570, AA0871, and AA07186 from the National Institutes of Health.

* To whom correspondence should be addressed. Phone: (215) 503-1614. Fax: (215) 923-2218. E-mail: Boris.Kholodenko@mail.tju.edu.

‡ Thomas Jefferson University.

§ Moscow State University.

|| GlaxoSmithKline.

[1] Abbreviations: EGF, epidermal growth factor; EGFR, EGF receptor; SH2, src homology 2 domain; PTB, phosphotyrosine-binding domain; Grb2, growth factor receptor binding protein 2; Shc, src homology and collagen domain protein; PLCγ, phosphoinositide-specific phospholipase C-γ; SOS, son of sevenless homologue protein; MAPK, mitogen-activated protein kinase; PI3K, phosphatidylinositol 3-kinase; GAP, GTPase-activating protein; SHP-1 and SHP-2, SH2 domain containing protein−tyrosine phosphatase-1 and -2; HRPO, horseradish peroxidase; PAGE, polyacrylamide gel electrophoresis.

10.1021/bi011506c CCC: $22.00
Published on Web 12/08/2001

that EGFR activation and subsequent phosphorylation of immediate downstream proteins developed shortly after addition of EGF with peak phosphorylation levels reached within the first 15 s of stimulation at 37 °C. However, in our previous experiments we were not able to resolve the initial rise of tyrosine phosphorylation of EGFR and its targets (*10*). The high-resolution monitoring of signaling responses is critical for better understanding of the underlying kinetic mechanisms and testing the model against the experiment. In the present paper we studied the rapid activation of the EGF receptor and downstream targets with 1 and 2 s resolution of the initial increase in tyrosine phosphorylation. In addition, we expanded the analysis to lower reaction temperatures (20 and 4 °C) and to longer time scales, ranging from 10 min at 37 °C to 1 h at 4 °C. Although temperature-induced changes in selected reaction rates involved in the EGFR pathway have been studied, the temperature dependence of the overall system responses has not been analyzed previously. Our experiments demonstrate that the temperature dependence of the signaling response patterns is not uniform. For instance, the time course of EGFR and PLCγ tyrosine phosphorylation remains transient over the entire temperature range examined, whereas the p85-PI3K phosphorylation response, transient at 37 °C, becomes more sustained at 20 and 4 °C, similar to a sustained Shc phosphorylation response.

Quantitative kinetic monitoring of the complex changes in EGF-induced signaling responses at different temperatures provides a rich data set for testing the kinetic model against the experiment. On the other hand, these experiments raise questions as to how the temperature-induced alterations in the overall response can be explained by the changes in individual compound reactions. A quantitative analysis can elucidate the differential control of the EGFR signaling pathway by compound processes. Since the data on the thermodynamic parameters of the compound reactions are incomplete, the model can be used to approach the reverse engineering problem of characterizing temperature-dependent alterations in the individual reaction rates based on experimentally measured systems responses. In this paper we have combined experimental and computational analyses of the temperature dependence of the overall cellular response to EGF. Computer simulations have been employed to analyze various feasible hypotheses regarding the temperature dependence of individual signaling processes. Our analysis demonstrates that the assumption of similar or identical activation energies (resulting in similar temperature coefficients, Q_{10}, for all reactions involved in the EGFR pathway) cannot account for the experimentally observed responses. Neither the assumption about predominant temperature-induced changes in the EGFR tyrosine kinase activity nor that in protein tyrosine phosphatase activities was sufficient to simulate the experimental data. We demonstrate the ability of our kinetic model to account *quantitatively* for temperature-induced changes in the overall signaling response based on differential temperature dependencies of different reaction groups, including receptor interactions with SH2 and PTB domain proteins, the EGFR tyrosine kinase, and protein tyrosine phosphatases. Interestingly, computer simulations suggest a dramatic decrease in the rates of EGFR dimerization and the membrane phosphatase of the receptor upon a change from 20 to 4 °C, which indicate that these reactions may be selectively affected by the phase transition in the lipid structures of the plasma membrane (*11*).

MATERIALS AND METHODS

Materials. Antibodies against EGFR (sheep polyclonal), PLCγ (mixed mouse monoclonals), and p85-PI3K (rabbit polyclonal) were obtained from Upstate Biotechnology Inc. (Lake Placid, NY); anti-Shc (rabbit polyclonal) was from Transduction Laboratories (Lexington, KY); anti-phosphotyrosine−agarose conjugates (mouse monoclonal) and protein G−Sepharose were obtained from Sigma Chemical Co. (St. Louis, MO); and HRPO-conjugated secondary antibodies and the Supersignal West Pico chemiluminescence substrate were from Pierce (Rockford, IL). All gels were obtained from Owl Separation Systems (Portmouth, NH), and nitrocellulose membranes were from Bio-Rad (Hercules, CA). Collagenase type 2 was from Worthington (Freehold, NJ); BSA fraction V and the "Complete" protease inhibitor cocktail were from Roche Molecular Biochemicals (Indianapolis, IN). Other chemicals and biochemicals were obtained from Sigma Chemical Co. (St. Louis, MO) or Fisher Scientific Co. (Pittsburgh, PA).

Cell Preparation and Incubation Conditions. Intact rat hepatocytes were isolated by collagenase perfusion as described previously (*12*). The hepatocyte isolation and incubation medium was a modified Krebs−Ringer bicarbonate buffer equilibrated with 95% O_2/5% CO_2 at pH 7.4, containing NaCl (120 mM), $NaHCO_3$ (25 mM), KCl (4.8 mM), $MgCl_2$ (1.2 mM), potassium phosphate (1.2 mM), Hepes (10 mM, pH 7.4), and $CaCl_2$ (1 mM). After isolation cells were stored on ice until use. Irrespective of the temperature of the final incubation, cells were preincubated for 40 min at 37 °C in a shaking water bath in capped plastic flasks in a gas phase of 95% O_2/5% CO_2 at a cell density of 10^7 cells/mL in the Krebs−Ringer bicarbonate incubation medium described above. For the longer term incubations (reaction periods >30 s), the incubation flasks were transferred to a shaking water bath maintained at the appropriate temperature (37, 20, or 4 °C), and after a 10 min temperature equilibration, reactions were started by the addition of EGF (20 nM). Reactions were stopped by removing 0.5 mL samples from the incubation flask at appropriate times and immediately mixing these with an equal volume of ice-cold 2× lysis buffer. The lysis buffer contained (final concentrations) lithium dodecyl sulfate (LDS) (0.2%), LiCl (50 mM), Hepes (25 mM, adjusted to pH 7.4 with LiOH), Li-EGTA (2.5 mM), glycerol (10%), Triton X-100 (1%), LiF (10 mM), activated sodium orthovanadate (0.2 mM), β-glycerophosphate (10 mM), dithiothreitol (10 μM), and Complete protease inhibitor cocktail (1 tablet per 50 mL of buffer).

Initial rates of EGF-induced signaling reactions were analyzed in parallel incubations carried out in 20 mL plastic scintillation vials equipped with a Teflon stir bar, positioned on a magnetic stir plate in a water bath maintained at the appropriate temperature. A sample (1.25 mL) of the preincubated cell suspension was transferred to the incubation vial, and after a 10 min temperature equilibration, reactions were started by the rapid addition of EGF (final concentration 20 nM, from a stock solution of 2.5 mM), followed, after reaction periods of 1−10 s, by 3 volumes of ice-cold 1.33×

lysis buffer. Control incubations in which a 5 μL volume of a color reagent was added established that mixing was essentially instantaneous (<0.5 s). A test of various lysis media demonstrated that the lysis buffer containing 0.2% dodecyl sulfate was effective in stopping the reaction sufficiently rapidly to enable resolution of the initial rate of EGFR autophosphorylation. Lithium salts were used in the lysis buffer because of the higher solubility of LDS compared to SDS at low temperature.

Lysates were kept on ice for up to 30 min, centrifuged in the cold (5 min), and either analyzed immediately or stored at −70 °C until use.

Immunoprecipitation Conditions, Gel Electrophoresis, and Western Blotting. Immunoprecipitations were carried out as described elsewhere (*10*). Briefly, 800 μg of LDS lysate protein was immunoprecipitated with 50 μL of anti-phosphotyrosine−agarose at 4 °C with constant mixing. Incubations were continued for 3−5 h, after which samples were spun down and immunoprecipitates were washed twice with HNTG buffer containing Hepes (20 mM, pH 7.5), NaCl (150 mM), Triton X-100 (0.1%), glycerol (10%), sodium orthovanadate (0.2 mM), NaF (10 mM), and protease inhibitor cocktail. EGFR immunoprecipitates, used for normalization of EGFR protein content on immunoblots, were prepared with 400 μg of LDS lysate and 25 μg of anti-EGFR antibody. Protein G−Sepharose (25 μL) was added during the last hour to capture the immunocomplex. Control experiments established that the immunoprecipitation conditions were maximally effective.

Immunoprecipitates were dissolved in Laemmli buffer (10% glycerol, 1.5% SDS, 1.5% β-mercaptoethanol, 5 mM EDTA, 0.02% bromophenol blue) and placed in a boiling water bath for 5 min. Proteins were separated by SDS−PAGE on 4−15% gradient gels. Anti-phosphotyrosine immunoprecipitates were loaded side by side with anti-EGFR immunoprecipitates or full lysates diluted 1:5 with Laemmli buffer, as standards for the quantitative estimate of tyrosine phosphorylation of specific signaling proteins. After being electroblotted onto nitrocellulose membranes and blocked for 1 h at room temperature with 3% BSA in TBST (10 mM Tris, pH 8.0, 150 mM NaCl, 0.05% Triton X-100), the membranes were blotted with antibodies to EGFR, PLCγ, Shc, and p85-PI3K. Blots were analyzed by enhanced chemiluminescence (Pierce Supersignal) using a Kodak CCF440 image analyzer, and each phosphorylated protein was expressed as a fraction of the total amount of that protein detected on the same membrane.

Kinetic Analysis. (A) Model of the EGFR Signaling Pathway. A detailed model of the EGFR signaling pathway is published elsewhere (*10*). Briefly, it describes the activation, dimerization, and tyrosine phosphorylation of EGFR, followed by the binding and activation/phosphorylation of adapter/target proteins, such as Shc, PLCγ, Grb2 (which binds to the receptor both directly and through phosphorylated Shc), and SOS (through Grb2). There are other signaling proteins that bind to EGFR in hepatocytes, e.g., the p85 subunit of PI3K, Ras-GAP, Eps15, GAB, and Src, and additional, as yet uncharacterized target proteins may exist. Here, we extended this model to incorporate EGF-induced binding and subsequent tyrosine phosphorylation of p85-PI3K and also included an unspecified protein (X) in order to account for additional receptor−protein interactions (Figure 1A,C).

Emerging evidence indicates that tyrosine phosphatases (such as SHP-1 and SHP-2) associate with EGFR pathway signaling proteins (such as PLCγ and PI3K) not only after but also prior to growth factor stimulation (*13*−*15*). The present model accounts for such complexes, describing the phosphatase reaction in terms of a three-step mechanism that involves the formation of the enzyme complexes with both the phosphorylated and unphosphorylated forms of a target protein. Figure 1B illustrates this schematically, representing a typical cycle of binding and subsequent phosphorylation of a target protein by the EGFR kinase and a coupled cycle of dephosphorylation of that protein by specific tyrosine phosphatase. Steps c and a in the latter cycle correspond to the reversible binding of the unphosphorylated and phosphorylated protein, and step b represents the phosphate release (Figure 1B).

(B) Reaction Stoichiometry and Kinetic Equations. The quantitative computational model of the EGFR pathway presented here comprises 42 reactions shown schematically in Figure 1C (listed in Table 1). The time-dependent behavior of EGF-induced signaling is described by a set of mathematical equations known as chemical kinetic equations, which are generated according to the reaction stoichiometry. Thirteen moiety conservation relations derived from the stoichiometry include the total concentrations of EGF, EGFR, PLCγ, PI3K, Grb2, Shc, SOS, and X proteins and the tyrosine phosphatases TP_1, TP_2, TP_3, TP_4, and TP_5. Computer simulations of the EGFR signaling pathway were performed using the biochemical kinetics software packages Dbsolve (*16*) and SCAMP (*17*).

Kinetic Parameters. Thermodynamic Restrictions along Cyclic Pathways in the Kinetic Scheme. If a kinetic scheme includes cycles, in which the initial and final states are identical, the equilibrium constants of the reactions along any cycle satisfy so-called "detailed balance" relationships (see, e.g., refs *18* and *19*). These detailed balance relations require the product of the equilibrium constants along a cycle to be equal to 1, as at equilibrium the net flux through any cycle vanishes. Therefore, such relations decrease the number of independent rate constants in a kinetic model. The restrictions on the kinetic constants are

$$K_{d15}K_{d16}/(K_{d13}\cdot K_{d14}) = 1$$

$$K_{d19}K_{d23}/(K_{d24}\cdot K_{d27}) = 1$$

$$K_{d24}K_{d25}/(K_{d26}\cdot K_{d28}) = 1$$

$$K_{d16}K_{d29}/(K_{d27}\cdot K_{d28}) = 1$$

$$K_{d19}K_{d30}/(K_{d26}\cdot K_{d29}) = 1$$

The kinetic parameters used in the model are consistent with either measured or estimated values reported in the literature. We initially assumed the parameter values specified in ref *10*. The simulated time courses of activation demonstrated a good fit to the experimentally observed transient and sustained responses at 37 °C (*10*). We subsequently optimized the parameter values within

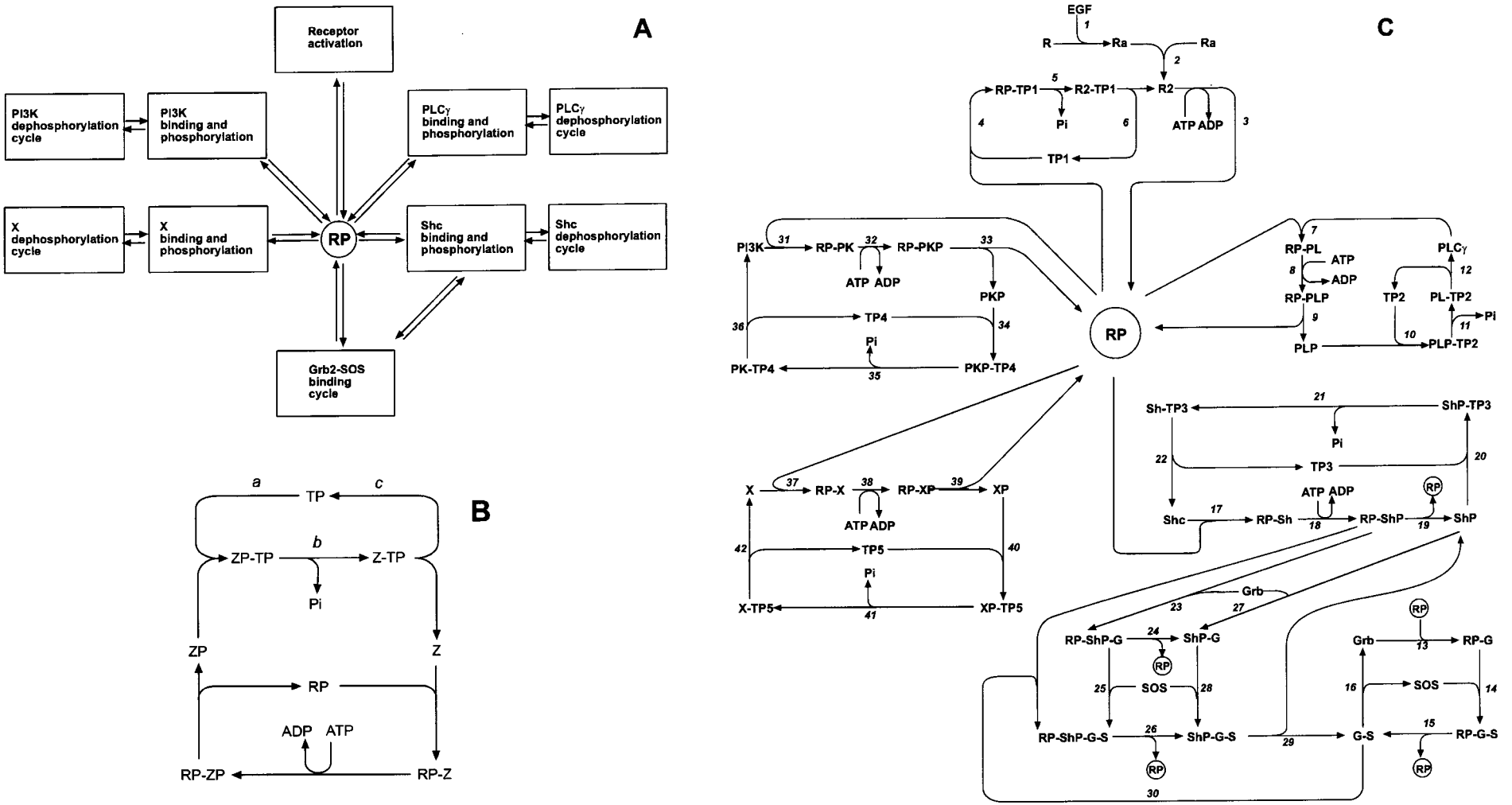

FIGURE 1: Schematic representation of the EGFR pathway. (A) Block diagram of EGFR signaling mediated by adapter and target proteins. (B) A typical cycle of binding and phosphorylation by EGFR of a target protein (Z) by the activated EGFR kinase (RP) and a coupled cycle of Z−P dephosphorylation by a specific tyrosine phosphatase (TP). All steps are reversible except step b. (C) Complete kinetic scheme of EGFR signaling mediated by adapter and target proteins. Numbering of individual steps is arbitrary. Designations: R, EGFR; R_a, EGFR−EGF; R_2, $(R_a)_2$; RP, tyrosine-phosphorylated EGFR (which is not complexed with adaptor/target proteins); TP_i ($i = 1, ..., 5$), specific tyrosine phosphatase i; RP-PL, RP-PLCγ; RP-PLP, RP-PLCγP; PLP, PLCγP; PL-TP_2, PLCγ-TP_2; PLP-TP_2, PLCγP-TP_2; RP-G, RP-Grb2; RP-G-S, RP-Grb2-SOS; G-S, Grb2-SOS; RP-Sh, RP-Shc; RP-ShP, RP-ShcP; ShP, ShcP; Sh-TP_3, Shc-TP_3; ShP-TP_3, ShcP-TP_3; RP-ShP-G, RP-ShcP-Grb2; ShP-G, ShcP-Grb2; RP-ShP-G-S, RP-ShcP-Grb2-SOS; ShP-G−S, ShcP-Grb2-SOS; RP-PK, RP-PI3K; RP-PKP, RP-PI3KP; PKP, PI3KP; PK-TP_4, PI3K-TP_4; PKP-TP_4, PI3KP-TP_4.

Table 1: Reactions and Kinetic Parameters[a]

reaction no.	bimolecular reactions	kinetic constants at 37 °C	
		k_{on} ($nM^{-1}\cdot s^{-1}$)	K_d (nM)
1	R + EGF = Ra	$k_1 = 3 \times 10^{-3}$	$K_{d1} = 20$
2	Ra + Ra = R_2	$k_2 = 0.011$	$K_{d2} = 74$
4	TP_1 + RP = RP-TP_1	$k_4 = 0.03$	$K_{d4} = 197$
6	RP-TP_1 = R_2 + TP_1	$k_{-6} = 5.1 \times 10^{-3}$	$K_{d6} = 26$
7	RP + PLCγ = RP-PL	$k_7 = 0.1$	$K_{d7} = 10$
9	RP-PLP = RP + PLP	$k_{-9} = 1.5 \times 10^{-4}$	$K_{d9} = 2000$
10	TP_2 + PLP = TP_2-PLP	$k_{10} = 1.5 \times 10^{-4}$	$K_{d10} = 10$
12	TP_2-PL = PLCγ + TP_2	$k_{-12} = 1 \times 10^{-5}$	$K_{d12} = 55$
13	RP + Grb = RP-G	$k_{13} = 1.5 \times 10^{-3}$	$K_{d13} = 133$
14	RP-G + SOS = RP-G-S	$k_{14} = 0.01$	$K_{d14} = 6$
15	RP-G-S = RP + G-S	$k_{-15} = 2.8 \times 10^{-3}$	$K_{d15} = 53$
16	G- = Grb + SOS	$k_{-16} = 1 \times 10^{-4}$	$K_{d16} = 15$
17	RP + Shc = RP-Sh	$k_{17} = 0.1$	$K_{d17} = 10$
19	RP-ShP = ShP + RP	$k_{-19} = 5 \times 10^{-4}$	$K_{d19} = 1406$
20	TP_3 + ShP = TP_3-ShP	$k_{20} = 5 \times 10^{-3}$	$K_{d20} = 19$
22	TP_3-Sh = Shc + TP_3	$k_{-22} = 2 \times 10^{-4}$	$K_{d22} = 50$
23	RP-ShP + Grb = RP-ShP-G	$k_{23} = 1.5 \times 10^{-3}$	$K_{d23} = 33$
24	RP-ShP-G = RP + ShP-G	$k_{-24} = 6.5 \times 10^{-4}$	$K_{d24} = 464$
25	RP-ShP-G + SOS = RP-ShP-G-S	$k_{25} = 0.015$	$K_{d25} = 2$
26	RP-ShP-G-S = ShP-G-S + RP	$k_{-26} = 1.1 \times 10^{-3}$	$K_{d26} = 464$
27	ShP + Grb = ShP-G	$k_{27} = 1 \times 10^{-3}$	$K_{d27} = 100$
28	ShP-G + SOS = ShP-G-S	$k_{28} = 0.03$	$K_{d28} = 2$
29	ShP-G-S = ShP + G-S	$k_{-29} = 0.035$	$K_{d29} = 14$
30	RP-ShP + G-S = RP-ShP-G-S	$k_{30} = 0.1$	$K_{d30} = 5$
31	RP + PI3K = RP-PK	$k_{31} = 0.1$	$K_{d31} = 20$
33	RP-PKP = RP + PKP	$k_{-33} = 0.047$	$K_{d33} = 974$
34	TP_4 + PKP = TP_4-PKP	$k_{34} = 7 \times 10^{-4}$	$K_{d34} = 10$
36	TP_4-PK = PI3K + TP_4	$k_{-36} = 8 \times 10^{-5}$	$K_{d36} = 12$
37	RP + X = RP-X	$k_{37} = 0.06$	$K_{d37} = 18$
39	RP-XP = RP + XP	$k_{-39} = 7 \times 10^{-5}$	$K_{d39} = 1500$
40	TP_5 + XP = TP_5-XP	$k_{40} = 6.9 \times 10^{-4}$	$K_{d40} = 46$
42	TP_5-X = X + TP_5	$k_{-42} = 1 \times 10^{-5}$	$K_{d42} = 30$

reaction no.	tyrosine phosphorylation and dephosphorylation steps	kinetic constants at 37 °C	
		k_f (s^{-1})	K_{eq} (nM)
3	R_2 = RP	$k_3 = 2.71$	$K_{eq3} = 100$
5	RP-TP_1 → R_2-TP_1	$k_5 = 7.44$	
8	RP-PL = RP-PLP	$k_8 = 10$	$K_{eq8} = 100$
11	TP_2-PLP → TP_2-PL	$k_{11} = 0.1$	
18	RP-Sh = RP-ShP	$k_{18} = 20$	$K_{eq18} = 100$
21	TP_3-ShP → TP_3-Sh	$k_{21} = 0.15$	
32	RP-PK = RP-PKP	$k_{32} = 9.85$	$K_{eq32} = 100$
35	TP_4-PKP → TP_4-PK	$k_{35} = 0.03$	
38	RP-X = RP-XP	$k_{38} = 10$	$K_{eq38} = 100$
41	TP_5-XP → TP_5-XP	$k_{41} = 1.3$	

[a] Total protein concentrations, which are assumed constant on the time scale under consideration, are the following (nM): $[EGFR]_{total} = 100$; $[EGF]_{total} = 680$; $[Shc]_{total} = 250$; $[PLC\gamma]_{total} = 150$; $[PI3K]_{total} = 50$; $[SOS]_{total} = 40$; $[Grb2]_{total} = 80$; $[X]_{total} = 220$; $[TP_1]_{total} = 100$; $[TP_2]_{total} = 450$; $[TP_3]_{total} = 250$; $[TP_4]_{total} = 125$; $[TP_5]_{total} = 210$. The concentrations of ATP, ADP, and P_i are assumed constant and do not enter the kinetic equations explicitly. Irreversible steps are shown by arrows. Designations of intermediates are given in the legend to Figure 1.

experimental or estimated constraints to minimize the square deviation of the residuals, $\sum(Res_i)^2$, where each residual (Res_i) is the difference between the experimental data point i and the value calculated by numerical integration of the model for the given parameter set. Table 1 lists the values of the kinetic parameters at 37 °C. The temperature dependence of the kinetic equations (constants) is described below.

Temperature Dependence of Compound Processes. (A) Protein−Protein Interactions. The rate of the association reaction between two proteins, P_1 and P_2, is described by mass action kinetics with the rate constants k_{on} and k_{off}. Expressing the k_{off} through the dissociation constant, K_d, as $k_{off} = k_{on}K_d$, the reaction rate (v) can be presented as

$$v = k_{on}([P_1][P_2] - K_d[P_1P_2]) \quad (1)$$

The dependence of a rate constant (k) on temperature (T) is given by the Arrhenius equation

$$d \ln k/dT = E_a/RT^2 \quad (2)$$

where E_a is the energy of activation, R is the gas constant, and T is the absolute temperature. Then, the ratio (q) of the k values at different temperatures, T_1 and T_2, is given by

$$q(T_1,T_2) = k(T_1)/k(T_2) = \exp(E_a(T_1 - T_2)/RT_2T_1) \quad (3)$$

The temperature dependence of the rate constants k_{on} and k_{off} is described by the activation energies E_{on} and E_{off}, respectively. The dependence of the equilibrium association constant ($K_a = k_{on}/k_{off}$) on temperature is determined by the enthalpy (ΔH) of the reaction, according to the van't Hoff equation

$$d \ln K_a/dT = \Delta H/RT^2 \quad (4)$$

where the enthalpy $\Delta H = E_{on} - E_{off}$. Accordingly, the ratio (q_d) of the K_d values at different temperatures, T_1 and T_2, can be expressed as

$$q_d(T_1,T_2) = K_d(T_1)/K_d(T_2) = \exp(-\Delta H(T_1 - T_2)/RT_1T_2) \quad (5)$$

If the kinetic constants, k_{on} and K_d, are known at temperature T_1, eqs 3 and 5 can be used to express the reaction rate at temperature T_2 as

$$v(T_2) = k_{on}(T_1)\exp(-E_{on}(T_1 - T_2)/RT_1T_2)([P_1][P_2] - K_d(T_1)\exp(\Delta H(T_1 - T_2)/RT_1T_2)[P_1P_2]) \quad (6)$$

Note that the rates of bimolecular interactions are presented in terms of the association rate constant (k_{on}) and the dissociation equilibrium constant (K_d) regardless of whether in the kinetic scheme depicted in Figure 1 the forward reaction is the association or dissociation step (see also Table 1). Accordingly, the temperature dependence is described by the E_{on} and q_{on} values for the k_{on}, and the ΔH and q_d values are used for the K_d (see Table 2 in the Results section).

Several groups have recently used isothermal titration calorimetry and surface plasmon resonance measurements to characterize thermodynamic parameters of various SH2 domain-mediated interactions with phosphotyrosine (pY) residues (*20*−*24*). The SH2 domain−pY interaction is stabilized by hydrogen bonds and appeared to be exothermic. The reported enthalpy (ΔH) of binding ranged from −7 to −10 kcal·mol^{-1}.

The equations above (eqs 3, 5, and 6) disregard changes in the activation energies and enthalpies with temperature. However, in thermodynamic studies of the binding of SH2 domains to the pY residues such changes have been reported. For instance, for the binding of a phosphotyrosine peptide from Shc (pY317) to the SH2 domain of Grb2, the following enthalpy (ΔH) and entropy (ΔS) changes with temperature (T) were detected: $\Delta H \sim -9.9$ kcal·mol^{-1}, $T\Delta S \sim -0.4$ kcal·mol^{-1} at 35 °C and $\Delta H \sim -7$ kcal·mol^{-1}, $T\Delta S \sim 1.9$

kcal·mol^{-1} at 15 °C (*23*). The enthalpy and entropy of binding are related to the standard free energy (ΔG) of the reaction:

$$\Delta G = \Delta H - T\Delta S \quad (7)$$

Since both ΔH and $T\Delta S$ increased with a temperature decrease, the resulting changes in the free energy were less than the corresponding changes in the enthalpy, ($\Delta G \sim 9.4$ and 8.9 kcal·mol^{-1} at 35 and 15 °C, respectively). In another example, an increase in the negative enthalpies for the binding of the Src SH2 domain to a series of phosphotyrosine peptides with a T decrease from 35 to 4 °C was characterized by modest heat capacity changes (0.1−0.2 kcal·mol^{-1}·deg^{-1}), whereas the ΔG values were relatively invariant with temperature (*24*).

When the dependence of the activation energy and entropy on temperature cannot be neglected, eqs 3 and 5 are no longer valid. In this case, the ratio, $q(T_1,T_2)$, of the kinetic constant at different temperatures is expressed in a more complex manner, which takes into account the changes in the thermodynamic parameters, E_{on}, ΔS_{on}, ΔH, and ΔS, which were disregarded in eqs 3 and 5. Our method, based on the evaluation of the goodness of fit for various kinetic constants, cannot resolve all of these thermodynamic parameters, because the same value for the ratio, q, can be obtained with different thermodynamic parameters. Therefore, we characterize temperature-dependent alterations in the individual reaction rates in terms of the ratios q_{on} and q_d and also in terms of the E_{on} and ΔH values as given by the Arrhenius and van't Hoff equations (see Table 2). Note that the phenomenological factors, q, used here are similar to the temperature coefficient Q_{10} (the factor by which the reaction rate increases on raising the temperature by 10 °C). Therefore, the kinetic constant ratios, q_{on} and q_d, will hereafter be referred to as the temperature coefficients.

(B) Tyrosine Phosphorylation Reactions. Since the ATP concentration in vivo is much higher than the Michaelis constant of the EGFR kinase for ATP (*25*, *26*), tyrosine phosphorylation of the receptor and its bound targets is described as pseudo-first-order reactions. When the kinetic constants k and the equilibrium constant K_{eq} are known at temperature T_1, the phosphorylation rate (v) of a protein (X) is expressed at temperature T_2 as

$$v(T_2) = k(T_1)\exp(-E_a(T_1 - T_2)/RT_1T_2)([X] - \exp(\Delta H(T_1 - T_2)/RT_1T_2)[XP]/K_{eq}(T_1)) \quad (8)$$

Given the standard free energy differences of the tyrosine phosphorylation reactions and the ATP/ADP ratio in vivo, the phosphorylation reactions appeared to be far from thermodynamic equilibrium, and the equilibrium constants (K_{eq}) are in the order of 10^2−10^3 at 37 °C (*10*). Consequently, in the temperature range under study, temperature-induced changes in the K_{eq} of tyrosine phosphorylation steps do not control the temporal pattern of signaling responses.

(C) Phosphatase Reactions. The phosphatase reactions are considered (kinetically) irreversible, given the measured ΔG values. The phosphatases are assumed to follow a Michaelis−Menten mechanism (*27*, *28*), and the concentration of inorganic phosphate is considered constant. For the three-step mechanism of dephosphorylation depicted in Figure 1B, the phosphatase enzymatic parameters at (quasi) steady-state conditions, V_{max} and K_m for the phosphorylated (*XP*) protein, relate to the rate constants of the elementary steps (a, b, and c, Figure 1B) as follows (*29*):

$$V_{max} = k_b k_c[TP]_{total}/(k_b + k_c); \qquad K_m = \frac{k_c(k_{-a} + k_b)}{k_a(k_b + k_c)} \quad (9)$$

where $[TP]_{total}$ is the total phosphatase concentration. Under conditions where phosphate release (step b) limits the overall reaction (i.e., $k_b \ll k_c$ in eq 9), the temperature dependence of V_{max} is determined by the activation energy of step b. However, the results of parameter optimization employed to fit experimental data at 37 °C demonstrated that the release of the unphosphorylated protein (step c) can significantly limit the dephosphorylation reaction, and its activation energy can determine the temperature dependence of V_{max}. Equations 2−4 and 9 demonstrate that the temperature dependence of the ratio V_{max}/K_m is characterized by the activation energy and enthalpy of the binding of the phosphorylated protein to the enzyme and the activation energy of the phosphate release. The available data assess the binding enthalpy for tyrosine−protein phosphatase 1B for artificial ligands to be in the range of −4 to −6 kcal·mol^{-1} (*30*) and the activation energy for the low molecular weight tyrosine−protein phosphatase (EC 3.1.3.2) to be about 14 kcal·mol^{-1} (*31*). For serine/threonine phosphatases (MAPP, SMP-1, II and IV, PP1c, PP2Ac, and calcineurin), the activation energies appeared to be in the range of 28−12 kcal·mol^{-1}, and a decrease in the V_{max}/K_m ratio by a 10° C temperature decrease was found to be in the range of 1.5−2.7 (*32*).

(D) Initial Conditions. In all simulations, the system was allowed to equilibrate in the absence of EGF. In particular, the complexes of the tyrosine phosphatases and EGFR target proteins were preformed in the absence of EGF (steps 12, 22, 36, and 42 in Figure 1C). Also Grb2 associates with SOS in the absence of EGF (*33*).

RESULTS

Early Kinetics of EGF-Induced Signaling Responses in Isolated Hepatocytes. The time course of the cellular response to EGF was followed in freshly isolated hepatocytes by measuring tyrosine phosphorylation of signaling intermediates after stimulation with 20 nM EGF. Tyrosine phosphorylated proteins were immunoprecipitated using an anti-PY antibody, and membranes were probed by Western blotting using anti-EGFR, anti-Shc, anti-PLCγ, or anti-PI3K antibody, respectively, for detection. The amount of phosphorylated protein detected in the phosphotyrosine immunoprecipitates was compared with the total protein detected in lysates or in protein immunoprecipitates obtained with an appropriate anti-protein antibody and analyzed in parallel on the same gels. These experiments provided estimates of each EGFR pathway phosphorylated protein as a fraction of the total protein in the lysate.

In our previous studies of EGF-induced signaling in isolated hepatocytes (*10*), the peak response of receptor autophosphorylation and activation of downstream signaling proteins was obtained at 15 s, the earliest time point studied, and the initial kinetics of the reactions could not be analyzed. A better characterization of the onset kinetics of the signaling

reactions would greatly enhance the reliability of the computational analysis. We modified the incubation conditions to obtain better resolution of the initial rate of the signaling reactions by rapid addition of EGF and lysis buffer (see Methods). In addition, we used a lysis buffer containing LDS (0.5%) plus Triton X-100 (0.5%), which caused rapid cell lysis. With these modifications, a temporal resolution of the order of seconds could be obtained, sufficient to capture the initial rate of EGFR autophosphorylation at 37 °C and resolve its onset kinetics from the activation of downstream signaling steps, including phosphorylation of Shc, PLCγ, and PI3K. Incubations at lower reaction temperatures, 20 and 4 °C, further facilitated the resolution of the early kinetics of these reactions. Figure 2A−C illustrates these early phosphorylation responses of EGFR and its targets. EGFR autophosphorylation reached a maximum (40−50% of total EGFR protein in these experiments) in 5−10 s at 37 °C, whereas downstream tyrosine phosphorylation reaction peaked after 10−20 s. At lower reaction temperatures, the initial rate of the reactions was decreased, and a distinct lag in the onset of downstream protein phosphorylation could be detected relative to the onset of EGFR autophosphorylation. At 20 °C, EGFR autophosphorylation peaked after 10−15 s and after 120−180 s at 4 °C, but the maximum level of phosphorylation was relatively unaffected by the temperature shift. Similarly, phosphorylation of Shc, PLCγ, and PI3K was delayed at the lower temperatures but reached peak levels almost equivalent to those obtained at 37 °C.

Kinetics of the Approach to a Quasi-Steady-State Condition. In a second series of experiments (Figure 2D−F) cells were incubated for more prolonged periods (up to 10, 20, or 60 min, depending on temperature) in order to analyze the kinetics of the approach to steady-state conditions after stimulation with a saturating concentration of EGF. In these experiments, a notable feature is the transient nature of the phosphorylation of EGFR, PLCγ, and PI3K, but not SHC, despite continuous stimulation with EGF. Lowering the reaction temperature markedly decreased the rate of decline of EGFR and PI3K phosphorylation and resulted in a relative elevation of the steady-state phosphorylation at lower temperatures. By contrast, PLCγ phosphorylation was transient even at low temperatures. These data suggest that the reactions that determine the transient response characteristics are differentially sensitive to changes in temperature.

It is of note that the peak phosphorylation state of EGFR expressed as a fraction of total EGR protein detected in the lysate varied between individual experiments and ranged from approximately 40% to 75−80% (e.g., compare panels A−C and D−F in Figure 2). These variations appeared to reflect differences in cell preparations rather than analytical problems, since the results were consistent in individual experiments, and the data from individual experiments always were the result of repeated analysis. Most of the variability was evident in EGFR, whereas the downstream target proteins exhibited less fluctuation. A likely explanation is that the amount of accessible or reactive EGFR protein represents a variable fraction of total EGFR protein. This variation may at least in part reflect different degrees of EGFR protein expression on the cell surface following preincubation (*34*). For instance, in cells that were not preincubated, the EGF-responsive fraction was less than 10% of total cellular EGFR protein (data not shown). For the computational analysis, the responsive EGFR fraction was normalized, so that at saturating EGF concentrations the peak response represented the same constant fraction of accessible EGFR protein for each series of experiments at a given temperature. A further complication of the experimental data is represented by the fraction of phosphorylated EGFR protein (5−7% of total EGFR protein) that was detected in unstimulated cells. It is not entirely clear whether this represents EGFR protein, phosphorylated in the absence of EGF-induced receptor dimerization, e.g., by other tyrosine kinases (such as src) that may be constitutively active in unstimulated cells, or that a small fraction of EGFR protein that can dimerize and autophosphorylate in the absence of EGF, e.g., by being compartmentalized in restricted membrane domains. These EGF-independent background phosphorylation reactions were not considered explicitly in the kinetic model; therefore, in all computational analyses phosphorylated protein levels were corrected for the small contribution of phosphorylated proteins present in unstimulated cells.

Computational Analysis of the Temperature Dependence of EGFR Signaling. For the computational analysis of these experimental data, the expanded reaction scheme of Figure 1C was applied (see Methods). Figure 3 shows the computer-simulated response patterns at 37 °C overlaid on the experimental data of Figure 2. The estimates of protein phosphorylation of any of the proteins are assumed to represent the sum of all corresponding phosphorylated complexes (illustrated in Figure 1C and listed in the legend to Figure 3). The computational results show a remarkable fit to the experimental observations and could adequately account for both the initial rapid increase in tyrosine phosphorylation and the subsequent transient or sustained kinetic patterns for EGFR and all of its downstream target proteins. Kinetic parameter values were optimized to minimize the difference between computer-simulated and measured response patterns at 37 °C. Importantly, the optimized parameters appeared to be within the range of experimentally measured values obtained from the literature and did not differ significantly from the kinetic constants used in the previous model (Table 1). A distinction between transient and sustained phosphorylation patterns is accounted for by the computational model in terms of differential affinities of unphosphorylated and phosphorylated targets for EGFR and differential kinetic parameters of the phosphatases (e.g., V_{max} and the rate constant of the release of the unphosphorylated protein) that generate unphosphorylated forms of EGFR and its target proteins, Shc, PLCγ, and PI3K (see ref *10* and Table 1).

Many of the characteristic features of the kinetic response patterns change markedly when the temperature is decreased to 20 and 4 °C (see Figure 2). As noted above, with the exception of PLCγ, all reactions show a less transient response pattern and a higher steady-state level at lower temperatures. As the values of kinetic constants were selected to provide the "best" fit to the data at 37 °C, the question arises as to which changes in the reaction kinetics are responsible for observed alterations in the EGF-induced responses. An advantage of using kinetic modeling for understanding the experimental observations is the ease with which distinct hypotheses can be tested against the data. If

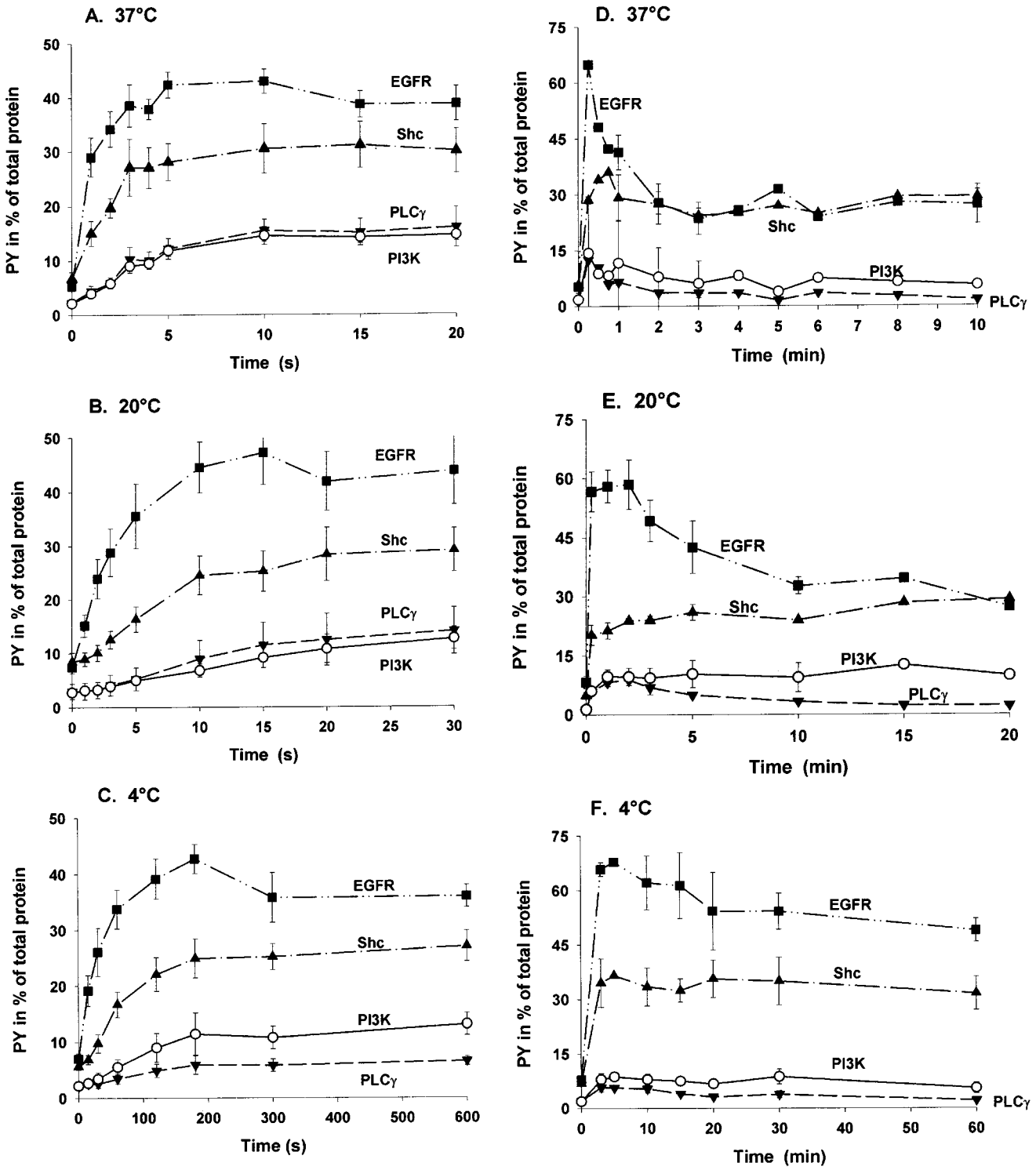

FIGURE 2: Time course of EGF-induced tyrosine phosphorylation at different temperatures. After preincubation at 37 °C for 40 min, hepatocyte suspensions were transferred to a water bath at the appropriate temperature (37, 20, or 4 °C) and stimulated with 20 nM EGF using incubation protocols for resolution of initial kinetics (A, 37 °C; B, 20 °C; C, 4 °C) or for longer term stimulation (D, 37 °C; E, 20 °C; F, 4 °C), as detailed in the Materials and Methods section. Cell lysates were analyzed for tyrosine-phosphorylated EGFR (■), Shc (▲), PLCγ1 (▼), and p85-PI3K (○) and expressed as a fraction of the total level of each protein in the lysate. Data shown are the mean ± SEM from six different experiments for the initial kinetics (A−C) and the mean ± range for two separate experiments for the longer term incubations (D−F). All analyses in each experiment were repeated two to four times and averaged.

the activation energies of compound processes were equal, then all of the rate constants would decrease proportionally with a temperature decrease [by a factor of $\exp(-E_a(T_1 - T_2)/RT_1T_2)$, see Methods, eq 3]. Since a simultaneous proportional decrease in all rate constants is equivalent to time scaling, the cellular response to EGF would simply develop more slowly at temperatures lower than 37 °C, and exactly the same levels of protein tyrosine phosphorylation would be reached during the longer time periods. As an illustration, panels A and B of Figure 4 present the response patterns for EGFR measured at 20 and 4 °C, respectively (filled squares), and computer-simulated responses (solid

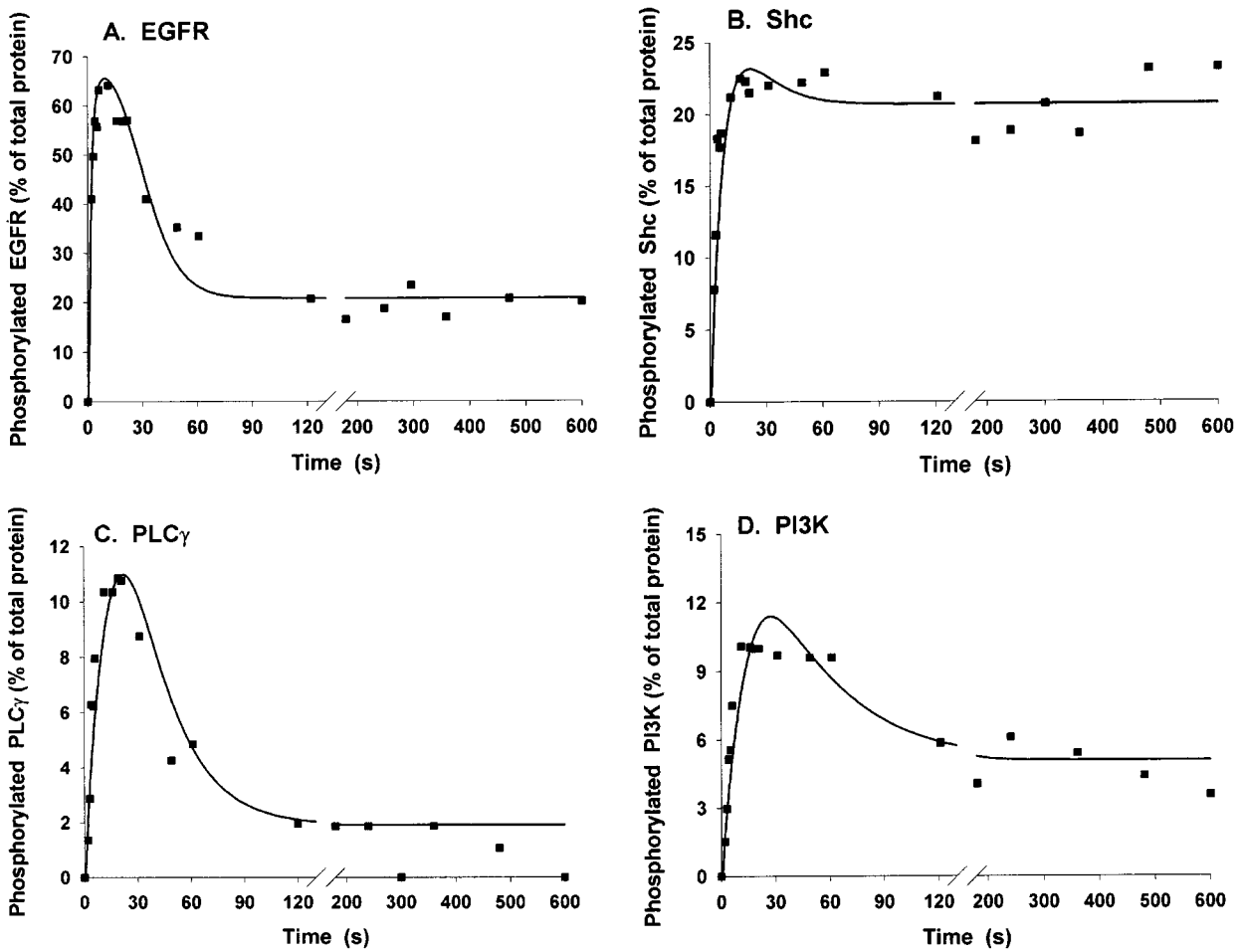

FIGURE 3: Computer simulation of EGF-induced signaling responses at 37 °C. The response patterns generated by a kinetic model presented in Figure 1C and Table 1 were overlaid on the experimental data shown in Figure 2. Data points were normalized and corrected for basal phosphorylation in unstimulated cells as discussed in the text. Phosphorylated proteins were calculated as the sums of the following complexes (see Figure 1): A, phosphorylated EGFR = 2([RP] + [RP-PLP] + [RP-ShP] + [RP-G] + [RP-G-S] + [RP-PL] + [RP-Sh] + [RP-ShP-G] + [RP-ShP-G-S] + [RP-PK] + [RP-PKP] + [RP-X] + [RP-XP] + [RP-TP_1]); B, phosphorylated Shc = [ShP] + [RP-Sh] + [RP-ShP-G] + [ShP-G] + [ShP-G-S] + [RP-ShP-G-S] + [ShP-TP_3]; C, phosphorylated PLCγ = [PLP] + [RP-PLP] + [PLP-TP_2]; D, phosphorylated PI3K = [PKP] + [RP-PKP] + [PKP-TP_4].

lines) calculated for E_a = 15 kcal·mol^{-1} (for comparison, the responses at 37 °C are shown by dashed lines). The selected value of 15 kcal·mol^{-1} ensured that the simulated and experimentally detected tyrosine phosphorylation levels of EGFR and its targets behave similarly at the rising segment of the corresponding response curves. However, panels A and B of Figure 4 make it evident that there is a systematic difference between the experimental EGFR responses and the computer simulations at the lower temperatures, although not so much in the early activation kinetics but in the peak levels and steady-state phosphorylation levels of EGFR. Comparable or even greater differences were observed for the downstream response patterns (data not shown). Clearly, the assumption of similar activation energies for all the reactions involved in the EGFR pathway cannot account for the experimentally observed kinetics.

The data of Figure 4 demonstrate that the assumption of uniform E_a resulted in an overestimate of the calculated peak EGFR phosphorylation level at temperatures of 20 and 4 °C compared to experimentally observed levels, and similar differences were observed for the peak phosphorylation of downstream EGFR target proteins, such as PLCγ and PI3K. This might suggest that the protein tyrosine kinases are preferentially affected by changes in temperature, compared to the phosphatase activities. Conversely, a predominant inhibition of the tyrosine phosphatases relative to EGFR kinase at lower temperatures could account for the observation that the experimentally observed rate of decay of phosphorylated EGFR is slower and the steady-state level of phosphorylation is higher, particularly at 4 °C. Therefore, we analyzed what changes in EGF-mediated responses would occur if the reactions catalyzed by the EGFR kinase and tyrosine phosphatases were differentially sensitive to a temperature decrease. As illustrated in Figure 5A, a preponderant temperature-induced decrease in the kinase activity (E_a = 15 kcal·mol^{-1}) compared to the tyrosine phosphatase (E_a = 5 kcal·mol^{-1}) results in the expected decline in peak and steady-state EGFR phosphorylation levels with temperature. Not surprisingly, a predominant sensitivity to the decrease in temperature of the phosphatase activities (E_a = 15 kcal·mol^{-1}) relative to EGFR kinase (E_a = 5 kcal·mol^{-1}) brings about qualitatively opposite changes in the phosphorylation response patterns (Figure 5B). Importantly, neither kinase nor phosphatase modulations slowed the kinetics of the descending phase of the EGFR transients. Hence, although temperature-induced changes in the tyrosine kinase and phosphatase activities strongly affect the protein phos-

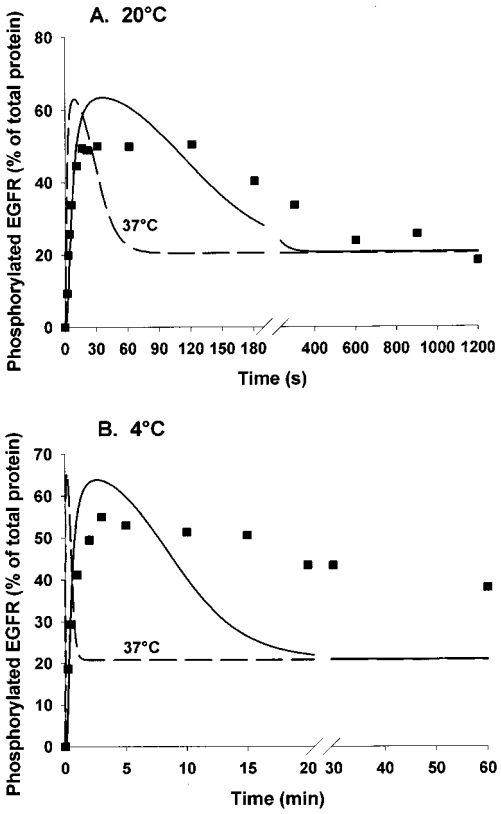

FIGURE 4: Simulation of EGFR autophosphorylation responses at 20 °C (A) and 4 °C (B) assuming identical activation energies of compound reactions. Computer-simulated EGFR phosphorylation responses (solid lines) were calculated on the basis of the kinetic constants resulting from the computational analysis at 37 °C (Figure 3) assuming equal activation energies, $E_a = 15$ kcal·mol^{-1}, for any reaction presented in Table 2. Experimental data (solid squares) were obtained from Figure 2, normalized for peak responses and corrected for background. Dashed lines show the response at 37 °C for comparison.

phorylation levels, they do not alter the characteristic transient time course of receptor phosphorylation and by themselves cannot account for the experimentally observed alterations of signaling responses.

The characteristic temporal pattern of tyrosine phosphorylation responses is determined by the progress of EGFR through cycles of interaction with its adapter/target proteins (Figure 1). The temperature dependence of these interactions has a major impact on the rate of decline of the phosphorylation state of EGFR and its downstream target proteins. For instance, computer simulations, which use the reported E_a and ΔH values of 15 kcal·mol^{-1} and -8 kcal·mol^{-1}, respectively, for all EGFR−adapter/target protein interactions (*20*−*24*), demonstrate a marked decline in the rate of EGFR phosphorylation at 20 and 4 °C but show significantly increased EGFR tyrosine phosphorylation levels compared to those observed at 37 °C (Figure 5C).

The analysis above illustrates how different temperature-induced changes in the compound reactions contribute to the temperature dependence of the overall responses to EGF stimulation. At the same time, none of the above simulations can *quantitatively* describe our experimental data. Therefore, we applied a computer-based approach of constrained parameter optimization to account for experimentally observed alterations in the signaling responses. We assumed that the temperature coefficients are similar within a group

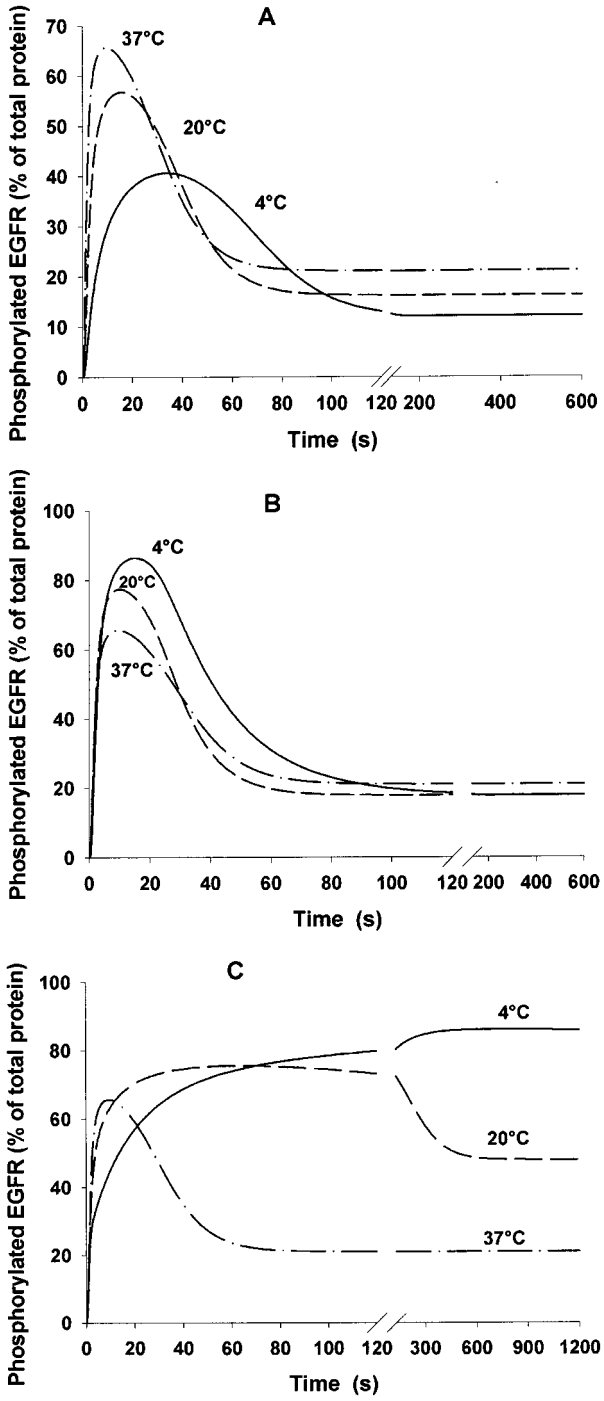

FIGURE 5: Alteration in simulated response patterns of EGFR phosphorylation with different assumptions regarding temperature sensitivity of compound processes. EGFR autophosphorylation responses were simulated on the basis of the kinetic constants of the computational analysis at 37 °C assuming a predominant decrease with temperature either in EGFR tyrosine kinase (A) or in protein tyrosine phosphatases (B). In (A), $E_a = 15$ kcal·mol^{-1} for steps 3, 8, 18, 32, and 38 and 5 kcal·mol^{-1} for steps 4−6, 10−12, 20−22, 34−36, and 40−42. In (B), $E_a = 5$ kcal·mol^{-1} for steps 3, 8, 18, 32, and 38 and 15 kcal·mol^{-1} for steps 4−6, 10−12, 20−22, 34−36, and 40−42. $E_a = 0$ for all other reactions. (C) Calculations used an identical value for $E_a = 15$ kcal·mol^{-1} and $\Delta H = -8$ kcal·mol^{-1} for all EGFR−adapter/target protein interactions; $E_a = \Delta H = 0$ for all other reactions. Dashed and solid lines correspond to the responses calculated at 20 and 4 °C, respectively (for comparison the responses at 37 °C are shown by dash-dot lines).

of reactions characterized by the same mechanism, as, for instance, for all SH2 domain-mediated interactions of un-

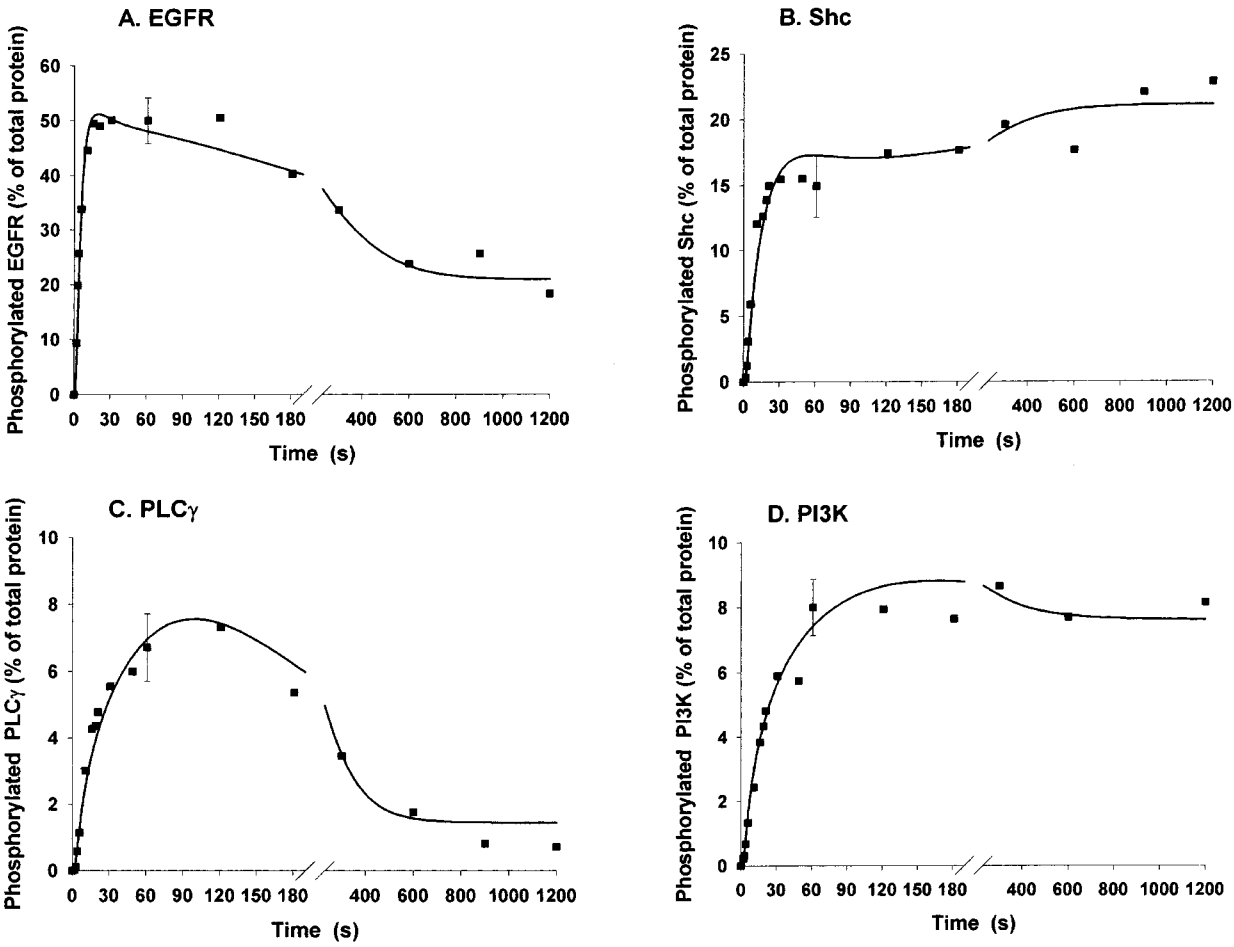

FIGURE 6: Best fit simulation of EGFR-mediated signaling at 20 °C. Experimental data points are derived from Figure 2B,E. Table 2 presents the thermodynamic parameters used in the calculations.

phosphorylated targets with the phosphorylated receptor. At the same time, we did not restrict potential distinctions in the temperature coefficients between different groups, such as between the phosphatase and kinase reactions. Assumed similarities in the thermodynamic parameters of reactions of the same type effectively decreased the number of unknown coefficients to the amount comparable with the number of experimentally measured response curves and, therefore, made it possible to estimate the coefficients within given constraints.

Signaling reactions comprising the initial part of the EGFR signaling pathway were conceptually divided into the following groups: (1) the SH2 domain-mediated reactions (such as PLCγ, Grb2, and PI3K interactions with EGFR and interaction of phosphorylated Shc with Grb2 or the Grb2−SOS complex); (2) interactions of Shc with EGFR, which involve both PTB and the SH2 domain (*3*); (3) the EGFR kinase catalyzed reactions; (4) reactions catalyzed by the phosphatases. In addition, interactions of EGFR with its target proteins were separated into two different groups depending on whether they occur prior to or after tyrosine phosphorylation of a target (see ref *10*). Figure 6 illustrates the ability of the model to give a good *quantitative* description of the measured response patterns at 20 °C. Importantly, computer simulations fit the data even when the temperature coefficients for various reactions within each group are identical, although the goodness of fit increases if the thermodynamic parameters can vary within a constrained range. Table 2 shows that the temperature coefficients, $q(37,20)$, which correspond to the best fit simulation, vary for different reaction groups. For instance, for the maximal activity of the EGFR kinase, the $q(37,20)$ value ranges from 1.04 to 1.5 depending on the target, whereas the temperature coefficients for the V_{max} of the phosphatases are found to be in the range from 2 to 6 (see Table 2 and eq 9). The temperature dependence of the association constants, k_{on}, for interactions of the EGF with unphosphorylated target proteins appears to be stronger than the dependence of the corresponding K_d values (i.e., $q_{on} > q_d$). This result is in line with recent findings that the free energy of the binding of the Src SH2 domain to various phosphotyrosine peptides did not change significantly between 35 and 4 °C (*24*). Interestingly, the temperature coefficient q_{on} appears to be less than q_d for phosphorylated target proteins, such as PLCγ, PI3K, and protein X, whereas q_{on} still slightly exceeds q_d for phosphorylated Shc (Table 2). Because of the differences in the temperature coefficients, the difference between the K_d values for unphosphorylated and phosphorylated target proteins (PLCγ, PI3K, and protein X) diminished with decreasing temperature, resulting in a more sustained EGFR phosphorylation and a decrease in the peak/steady-state ratio for phosphorylated EGFR.

The question arises if the responses observed at 4 °C can be described by the E_a and ΔH values that determine the coefficients q for the 37−20 °C temperature change. Substituting these parameters in the model, we found

Table 2: Temperature Dependence of Bimolecular Reactions and of Tyrosine Phosphorylation and Dephosphorylation Steps

(A) Bimolecular Reactions

	$T = 20$ °C				$T = 4$ °C			
reaction no.	E_{on} (kcal/mol)	q_{on} (37,20)	ΔH (kcal/mol)	q_d (37,20)	E_{on} (kcal/mol)	q_{on} (20,4)	ΔH (kcal/mol)	q_d (20,4)
1	15.86	4.44	−2.60	1.28	10.90	2.95	−2.60	1.29
2	16.40	4.68	1.37	0.88	30.31	20.18	0.34	0.97
4	0.40	1.04	−17.35	5.12	10.89	2.94	−11.46	3.12
6	15.89	4.46	−3.91	1.44	20.85	7.90	−5.89	1.79
7	14.41	3.88	−6.58	1.86	6.46	1.90	−6.87	1.98
9	7.12	1.95	−16.13	4.56	7.71	2.15	−11.78	3.22
10	4.37	1.51	−13.90	3.70	5.97	1.81	−14.93	4.39
12	15.89	4.46	−2.34	1.25	21.45	8.39	−7.30	2.06
13	18.39	5.64	−2.60	1.28	19.33	6.79	−2.60	1.29
14	14.41	3.88	−2.60	1.28	14.41	4.17	−2.60	1.29
15	14.41	3.88	−2.60	1.28	14.41	4.17	−2.60	1.29
16	13.42	3.54	−2.60	1.28	16.82	5.30	−2.60	1.29
17	14.05	3.75	−8.46	2.22	7.10	2.02	−13.43	3.78
19	6.86	1.91	−3.85	1.44	9.88	2.66	−9.79	2.64
20	1.05	1.10	−13.90	3.70	1.88	1.21	−17.87	5.88
22	7.94	2.11	4.01	0.62	16.88	5.33	0.86	0.92
23	18.39	5.64	−2.60	1.28	19.29	6.78	−2.60	1.29
24	14.41	3.88	−2.60	1.28	14.41	4.17	−2.60	1.29
25	14.41	3.88	−2.60	1.28	14.41	4.17	−2.60	1.29
26	14.41	3.88	−2.60	1.28	14.41	4.17	−2.60	1.29
27	18.39	5.64	−2.60	1.28	15.48	4.64	−2.60	1.29
28	14.41	3.88	−2.60	1.28	14.41	4.17	−2.60	1.29
29	14.41	3.88	−2.60	1.28	14.41	4.17	−2.60	1.29
30	14.41	3.88	−2.60	1.28	14.41	4.17	−2.60	1.29
31	16.34	4.65	−2.60	1.28	8.39	2.30	−2.60	1.29
33	5.13	1.62	−18.12	5.50	0.64	1.07	−13.77	3.92
34	0.40	1.04	−17.87	5.38	5.36	1.70	−17.87	5.88
36	6.95	1.92	1.95	0.83	14.89	4.38	3.96	0.61
37	19.38	5.64	−2.60	1.28	11.43	3.11	−2.60	1.29
39	3.39	1.18	−16.40	4.68	3.16	1.37	−20.70	7.78
40	0.40	1.04	−17.87	5.38	5.35	1.70	−17.87	5.88
42	9.93	2.54	3.02	0.75	13.30	3.74	1.04	0.90

(B) Tyrosine Phosphorylation and Dephosphorylation Steps[a]

	$T = 20$ °C				$T = 4$ °C			
reaction no.	E_a (kcal/mol)	q_f (37,20)	ΔH (kcal/mol)	q_{eq} (37,20)	E_a (kcal/mol)	q_f (20,4)	ΔH (kcal/mol)	q_{eq} (20,4)
3	0.40	1.04	1.09	0.90	3.83	1.46	1.09	0.90
5	22.29	8.15			31.23	22.11		
8	4.37	1.51	1.09	0.90	3.17	1.37	1.09	0.90
11	23.28	8.94			17.32	5.57		
18	4.37	1.51	1.09	0.90	2.63	1.30	1.09	0.90
21	16.11	4.56			21.08	8.09		
32	0.40	1.04	1.09	0.90	1.53	1.16	1.09	0.90
35	15.33	4.23			12.95	3.61		
38	4.37	1.51	1.09	0.90	2.80	1.32	1.09	0.90
41	17.32	5.10			23.28	10.06		

[a] Here, q_f and q_{eq} are the temperature coefficients for the forward rate constants and equilibrium constants, respectively.

qualitative agreement between computer simulations and measured response patterns, but there was significant deviation from the experimental values, suggesting that the temperature coefficients were not uniform throughout this temperature range. To reach *quantitative* equivalence, we assumed that the q values can vary for the 37−20 and 20−4 °C ranges but constrained the corresponding changes. Although this assumption improved the fit quality, a good quantitative description of the data could only be reached after a larger decrease in the rates of steps 2 and 5 was applied (Figure 7). The former step is the EGF receptor dimerization reaction, and the latter involves the release of inorganic phosphate in the receptor dephosphorylation reaction. Table 2 demonstrates that the k_{on} of step 2 and the rate constant (k_5) of phosphate release decrease by a factor of 20, when the temperature decreases from 20 to 4 °C (such a decrease in k_5 corresponds to a 14-fold decrease in V_{max} of the receptor phosphatase). We speculate that an accelerated decline in the rates of these particular reactions in the lower temperature range may be related to the phase transition in the membrane lipids, which occurs in the temperature range between 10 and 15 °C and which may affect both the dimerization step and the reaction catalyzed by a membrane-bound phosphatase (*11*). Since the apparent E_a of EGFR lateral diffusion was reported to be 6.1 kcal·mol^{-1} (*35*), which is too small to account for large changes in the k_{on}, we conclude that EGFR lateral diffusion does not limit EGFR dimerization (*36*).

DISCUSSION

The past decade has witnessed explosive growth in the amount of experimental work aimed to clarify structural, thermodynamic, and kinetic parameters of multiple interactions involved in receptor tyrosine kinase-mediated signaling. However, little effort has been directed at linking together various pieces of information to elucidate how integrative cellular responses to growth factors are influenced by alterations in the kinetics of component processes. This paper employs molecular level computational modeling to gain a better understanding of the experimentally measured temperature dependence of signaling responses to EGF in liver cells in terms of temperature-induced alterations in the kinetics of compound processes.

For the EGF receptor and its target proteins, we measured the progression of tyrosine phosphorylation with a time resolution of seconds that enabled us to resolve the rapid initial rise of the phosphorylation response of EGFR and several downstream target proteins following EGF stimulation. After the responses reached their peak level, the time interval between subsequent measurements was increased to follow a slower relaxation to a stationary level. The kinetics of EGFR-mediated signaling was followed at three different temperatures, 37, 20, and 4 °C. Data obtained at 37 °C were used to test a mechanistic model of EGF signaling, formulated in molecular terms as cascades of protein interactions that involve EGFR, Shc, PLCγ, PI3K, Grb2, and SOS proteins and phosphorylation/dephosphorylation reactions. Each molecular step of the model is a relatively simple biochemical process. Kinetic parameters were selected using information available from the extensive literature and adjusted when necessary within reported ranges to obtain a quantitative correspondence between computer-simulated and observed response patterns.

We have previously shown that the transient time course of receptor phosphorylation results from the protection of phosphotyrosine residues in the cytoplasmic domain against a constitutive phosphatase activity, as long as that residue is occupied by a target protein (*10*). At the same time, the transient pattern of tyrosine phosphorylation of PLCγ and PI3K is shaped by the kinetic properties of the phosphatases (cf. ref *8*). If the concentration of substrates for the phosphatase greatly exceeds that of the enzyme, the assumption of (quasi) steady-state conditions results in Michaelis−Menten kinetics. However, the concentrations of phospho-

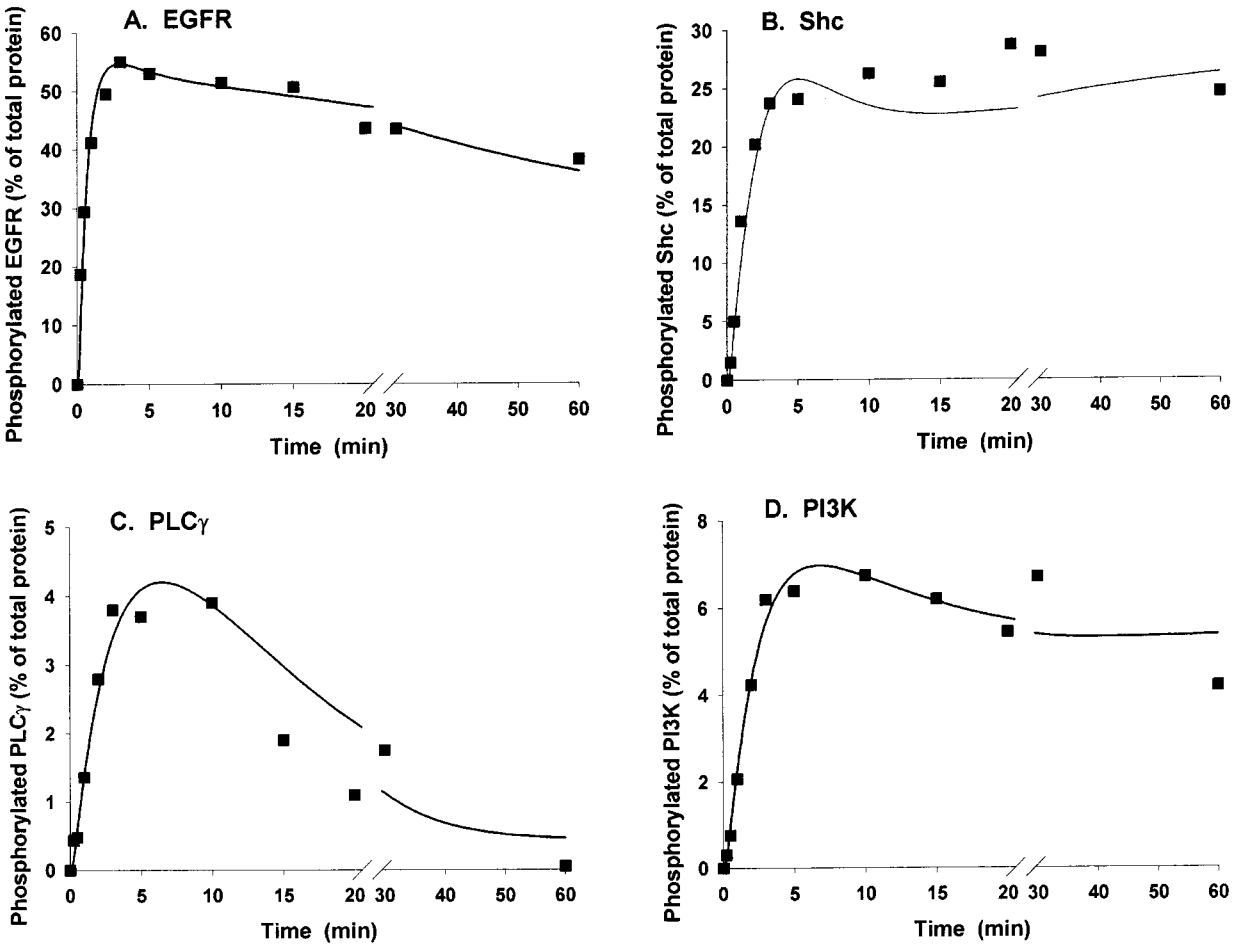

FIGURE 7: Best fit simulation of EGFR-mediated signaling at 4 °C. Experimental data points are derived from Figure 2C,F. Table 2 presents the thermodynamic parameters used in the calculations.

rylated EGFR and its target proteins appear to be in the same range as the estimated phosphatase concentrations (*38*, *39*). In addition, on the time scale of the rapid initial burst in receptor phosphorylation and accumulation of phosphorylated/activated target proteins, the steady-state assumption is not necessarily correct. Therefore, to account for rapid initial responses, the phosphatase reactions are described mechanistically at the level of the elemental steps (*40*, *41*). Our results demonstrate the critical role of the slow dissociation of the complexes formed by the phosphatases and unphosphorylated PLCγ and PI3K, respectively (Table 1, steps 12 and 36). Because steps 12 and 36 are readily reversible, these complexes can exist even before EGF stimulation. Indeed, the existence of such complexes between tyrosine phosphatases SHP-1 and SHP-2, and PLCγ and PI3K, has recently been reported in different cell types, including liver cells (*13*−*15*). Notably, in agreement with the reported data (*13*, *15*), computer simulations demonstrate that the concentrations of these complexes increase after EGF stimulation.

The integrated cellular response to EGF depends strongly on the reaction temperature. At 20 °C the characteristic time of tyrosine phosphorylation progression increased by a factor of approximately 2 for EGFR, 3 for Shc, and 4−5 for PLCγ. At 4 °C, the corresponding times for EGFR, Shc, and PLCγ tyrosine phosphorylation increased by factors of 6, 15, and 20, respectively, compared to those at 37 °C. After the maximum level was achieved, the time of the relaxation of EGFR and PLCγ phosphorylation to a sustained level increased from about 1 min at 37 °C to approximately 8−10 and 20 min at 20 and 4 °C, respectively. The data show that the temporal responses of the EGFR target proteins changed with temperature even more dramatically than the EGFR response. Using our kinetic model, we demonstrated that various a priori assumptions, e.g., the assumption of similar temperature dependencies for all the reactions involved in EGF-mediated signaling, cannot account for the temperature-induced alterations in the response patterns observed in our experiments. However, good *quantitative* agreement between computer-simulated and measured response patterns was obtained by assuming differential temperature coefficients for the rate constants for different reaction groups, such as SH2 and PTB domain-mediated interactions, phosphorylation of multiple targets by the EGFR kinase, and dephosphorylation of EGFR and its target proteins catalyzed by the phosphatases. The values obtained from the computational analysis for the temperature coefficients, q_{on} and q_d, indicate that upon the temperature decrease to 20 °C (or 4 °C) all bimolecular reactions exhibit a marked decrease in either the k_{on} or K_d values (Table 2A), implying that, for any protein−protein interaction involved in EGFR-mediated signaling, the dissociation rate constant k_{off} always decreases strongly upon the transition to lower temperatures. The rates of tyrosine phosphorylation reactions catalyzed by the EGFR kinase were described in the model by (pseudo) first-order rate constants given the values of the cellular ATP concen-

tration (in the order of millimolar) and the Michaelis constant for ATP (micromolar range). We found moderate temperature-induced changes in the maximal activities of these reactions (expressed by q_f in Table 2B) compared to corresponding changes in the V_{max} for the phosphatases (Table 2 and eq 9). Interestingly, large changes in both the V_{max} and K_m for the phosphatases result in moderate changes in the V_{max}/K_m ratio, which are comparable to the corresponding temperature-induced changes in the EGFR kinase (with a single exception for the V_{max}/K_m ratio of the receptor phosphatase at 4 °C; see above).

To accommodate additional EGFR interacting proteins that may respond to EGF stimulation, we incorporated a generic uncharacterized protein X into the model. There are multiple candidate proteins that could fit into this category, such as Eps15 involved in initiating endocytosis, soluble tyrosine kinases of the Src family, or adapter proteins such as GAB1/2 that may mediate additional cycles of activation of downstream signaling pathways. The kinetic constants describing the phosphorylation/dephosphorylation cycle of protein X that emerged from the modeling without further constraints were in the same range as those obtained for corresponding reactions in other cycles, such as PLCγ or Shc proteins. To test the model robustness, we excluded protein X and reoptimized the values of kinetic and thermodynamic parameters to minimize the deviation of simulated and experimental time courses. The simulated phosphorylation response patterns demonstrated essentially the same goodness of fit to experimental data. Not surprisingly, the total concentrations of the remaining signaling proteins, determined on the basis of the goodness of fit, *increased* in comparison with the values listed in Table 1. For instance, the abundance of Shc, Grb2, and PLCγ proteins increased by 50, 44, and 50 nM, respectively (the total X concentration was determined to be 220 nM in the original model). The changes in the rate constants were not significant, except for some reactions of the PLCγ cycle. Also, moderate changes were observed in the temperature coefficients of the reaction constants. Importantly, these changes did not compromise any of the conclusions made in this paper, indicating that the model has the capacity to accommodate additional EGFR−protein interactions without fundamentally affecting the results of these analyses.

This robustness of the kinetic model allowed us to incorporate mechanistically specific interactions involved in the EGFR signaling network, the elements of which are still open to debate. For instance, recent evidence indicates that phosphorylation of the p85 subunit of PI3K occurs indirectly, mediated by the adapter protein GAB2 (*15*). Alternatively, p85 phosphorylation may result from heterodimerization of EGFR with other ERB-family receptors, e.g., ERB-B3 (*37*). In our studies on rat hepatocytes, we detected only low levels of these proteins in EGFR immunoprecipitates. To what extent these or other indirect pathways are responsible for p85-PI3K phosphorylation as opposed to direct EGFR binding is therefore still unclear. With the proliferation of our knowledge of molecular mechanisms involved in the EGFR signaling network, further refinements of the present model will be required. Yet, the analysis of the model robustness suggests that additional components can be incorporated without affecting the basic conclusions and structure of the kinetic model.

Our kinetic model did not incorporate the processes of EGFR internalization and its degradation in lysosomes. At 37 and 20 °C we have studied responses to EGF stimulation during time periods up to 20 min, when the effects of EGFR internalization cannot be disregarded (*42*−*44*). No EGFR transfer to endosomes has been described at 4 °C (*45*). Yet, how can the kinetic description of the temperature dependence of EGFR signaling be successful over this entire temperature range, irrespective of whether EGFR endocytosis occurs or not? It has been shown that activated EGFR at the plasma membrane and in endosomes contributes equally to the phosphorylation of Shc and PLCγ [but not to the hydrolysis of the substrate of PLCγ phosphatidylinositol 4,5-bisphosphate (*6*, *46*)]. Moreover, the internalized receptor continues to signal and effectively participates in Ras activation (*46*). In agreement with these experimental findings, our computations show that the signaling response patterns can be quantitatively described by similar temperature coefficients upon changes from 37 to 20 °C and from 20 to 4 °C with the exception of large changes in steps 2 and 5, which presumably are associated with the plasma membrane phase transition that occurs in the temperature range of 10−15 °C.

In summary, this study strongly supports the validity of the kinetic model description of the EGFR-mediated signaling and suggests that the integrated network analysis provides an effective tool to help to identify how specific steps in the signaling pathways can account for disturbances in the overall response of the system.

REFERENCES

1. Carpenter, G. (1992) *FASEB J. 6*, 3283−3289.
2. Schlessinger, J. (1994) *Curr. Opin. Genet. Dev. 4*, 25−30.
3. Pawson, T. (1995) *Nature 373*, 573−580.
4. Schlessinger, J. (2000) *Cell 103*, 211−225.
5. Schlessinger, J., and Bar-Sagi, D. (1994) *Cold Spring Harbor Symp. Quant. Biol. 59*, 173−179.
6. Haugh, J. M., Schooler, K., Wells, A., Wiley, H. S., and Lauffenburger, D. A. (1999) *J. Biol. Chem. 274*, 8958−8965.
7. Roche, S., Koegl, M., and Courtneidge, S. A. (1994) *Proc. Natl. Acad. Sci. U.S.A. 91*, 9185−9189.
8. Haugh, J. M., and Lauffenburger, D. A. (1998) *J. Theor. Biol. 195*, 187−218.
9. Bhalla, U. S., and Iyengar, R. (1999) *Science 283*, 381−387.
10. Kholodenko, B. N., Demin, O. V., Moehren, G., and Hoek, J. B. (1999) *J. Biol. Chem. 274*, 30169−30181.
11. McCallum, C. D., and Epand, R. M. (1995) *Biochemistry 34*, 1815−1824.
12. Hoek, J. B., Thomas, A. P., Rubin, R., and Rubin, E. (1987) *J. Biol. Chem. 262*, 682−691.
13. Takahashi, Y., Akanuma, Y., Yazaki, Y., and Kadowaki, T. (1999) *J. Cell Physiol. 178*, 69−75.
14. Machide, M., Kamitori, K., and Kohsaka, S. (2000) *J. Biol. Chem. 275*, 31392−31398.
15. Kong, M., Mounier, C., Wu, J., and Posner, B. I. (2000) *J. Biol. Chem. 275*, 36035−36042.
16. Goryanin, I., Hodgman, T. C., and Selkov, E. (1999) *Bioinformatics 15*, 749−758.
17. Sauro, H. M. (1993) *Comput. Appl. Biosci. 9*, 441−450.
18. Kholodenko, B. N., Schuster, S., Garcia, J., Westerhoff, H. V., and Cascante, M. (1998) *Biochim. Biophys. Acta 1379*, 337−352.
19. Hearon, J. Z. (1953) *Bull. Math. Biophys. 15*, 121−141.
20. Lemmon, M. A., and Ladbury, J. E. (1994) *Biochemistry 33*, 5070−5076.
21. Ladbury, J. E., Lemmon, M. A., Zhou, M., Green, J., Botfield, M. C., and Schlessinger, J. (1995) *Proc. Natl. Acad. Sci. U.S.A. 92*, 3199−3203.

22. Ladbury, J. E., Hensmann, M., Panayotou, G., and Campbell, I. D. (1996) *Biochemistry 35*, 11062−11069.
23. McNemar, C., Snow, M. E., Windsor, W. T., Prongay, A., Mui, P., Zhang, R., Durkin, J., Le, H. V., and Weber, P. C. (1997) *Biochemistry 36*, 10006−10014.
24. Bradshaw, J. M., Grucza, R. A., Ladbury, J. E., and Waksman, G. (1998) *Biochemistry 37*, 9083−9090.
25. Posner, I., Engel, M., and Levitzki, A. (1992) *J. Biol. Chem. 267*, 20638−20647.
26. Posner, I., and Levitzki, A. (1994) *FEBS Lett. 353*, 155−161.
27. Dechert, U., Adam, M., Harder, K. W., Clark-Lewis, I., and Jirik, F. (1994) *J. Biol. Chem. 269*, 5602−5611.
28. Zhang, Z. Y., Walsh, A. B., Wu, L., McNamara, D. J., Dobrusin, E. M., and Miller, W. T. (1996) *J. Biol. Chem. 271*, 5386−5392.
29. Cornish-Bowden, A. (1995) *Fundamentals of Enzyme Kinetics*, Portland Press, London.
30. Zhang, Y. L., Yao, Z. J., Sarmiento, M., Wu, L., Burke, T. R., and Zhang, Z. Y. (2000) *J. Biol. Chem. 275*, 34205−34212.
31. Zhang, Z. Y., and VanEtten, R. L. (1991) *J. Biol. Chem. 266*, 1516−1525.
32. Mitsui, T., Kitazawa, T., and Ikebe, M. (1994) *J. Biol. Chem. 269*, 5842−5848.
33. Chook, Y. M., Gish, G. D., Kay, C. M., Pai, E. F., and Pawson, T. (1996) *J. Biol. Chem. 271*, 30472−30478.
34. Gladhaug, I. P., and Christoffersen, T. (1987) *Eur. J. Biochem. 164*, 267−275.
35. Hillman, G. M., and Schlessinger, J. (1982) *Biochemistry 21*, 1667−1672.
36. Tanner, K. G., and Kyte, J. (1999) *J. Biol. Chem. 274*, 35985−35990.
37. Russel, W. E., and Robert, S. C. (1998) The EGF/TGFa family of growth factors and their receptors, in *Liver Growth and Repair* (Strain, A. J., and Diehl, A. M., Eds.) pp 185−218, Chapman and Hall, London.
38. Tonks, N. K., Diltz, C. D., and Fischer, E. H. (1988) *J. Biol. Chem. 263*, 6722−6730.
39. Zhang, Z. Y. (1997) *Curr. Top. Cell Regul. 35*, 21−68.
40. Kholodenko, B. N., and Westerhoff, H. V. (1995) *Trends Biochem. Sci. 20*, 52−54.
41. Ferrell, J. E., Jr., and Bhatt, R. R. (1997) *J. Biol. Chem. 272*, 19008−19016.
42. Vieira, A. V., Lamaze, C., and Schmid, S. L. (1996) *Science 274*, 2086−2089.
43. Wang, Z., and Moran, M. F. (1996) *Science 272*, 1935−1939.
44. Emlet, D. R., Moscatello, D. K., Ludlow, L. B., and Wong, A. J. (1997) *J. Biol. Chem. 272*, 4079−4086.
45. Goldstein, J. L., Anderson, R. G., and Brown, M. S. (1979) *Nature 279*, 679−685.
46. Haugh, J. M., Huang, A. C., Wiley, H. S., Wells, A., and Lauffenburger, D. A. (1999) *J. Biol. Chem. 274*, 34350−34360.

BI011506C